Simulations of Turbulence Transport with Kinetic Electrons and Electromagnetic Effects from the Summit Framework

Y. Chen 1), S. E. Parker 1), B. I. Cohen 2), A. M. Dimits 2), W. M. Nevins 2), D. Shumaker 2), V. K. Decyk 3) and J. N. Leboeuf 3)

1) Univ. of Colorado, Boulder, Colorado, USA
2) Lawrence Livermore National Laboratory, Livermore, California, USA
3) Univ. of California, Los Angeles, California, USA

email contact: yang.chen@colorado.edu

Abstract. A new electromagnetic kinetic electron simulation model that uses a generalized split-weight scheme, where the adiabatic part is adjustable, along with a parallel canonical momentum formulation has been developed in three-dimensional toroidal flux-tube geometry. This model includes electron-ion collisional effects and has been linearly benchmarked. It is found that for H-mode parameters, the nonadiabatic effects of kinetic electrons increase linear growth rates of the Ion-Temperature-Gradien-Driven (ITG) modes, mainly due to trapped-electron drive. The ion heat transport is also increased from that obtained with adiabatic electrons. The linear behavior of the zonal flow is not significantly affected by kinetic electrons. The ion heat transport decreases to below the adiabatic electron level when finite plasma β is included due to finite-β stabilization of the ITG modes. This work is being carried out using the "Summit Framework." Progress on Summit, an open-source framework for both local and global massively parallel gyrokinetic turbulence simulations with kinetic electrons and electromagnetic perturbations, is reported.

1 Introduction

Kinetic electron physics is currently a primary challenge in the simulation of magnetic fusion turbulence and transport. Until recently, the vast majority of three-dimensional gyrokinetic particle simulations with realistic geometry have used the adiabatic electron approximation [1, 2, 3, 4]. The difficulty with a fully kinetic treatment of electrons in gyrokinetic particle simulations using the δf-method arises from the fact that for typical tokamak plasmas, where

the electron and ion temperatures are of similar magnitude, the electrons move a factor of $\sim \sqrt{m_i/m_e}$ (m_i and m_e are the masses of the ion and the electron) faster than the ions along the magnetic field. This poses a stringent constraint on the time step, the Courant condition $k_\parallel v_{\rm Te} \triangle t \leq 1$. To overcome this constraint a new kinetic electron model that uses a generalized split-weight scheme [5], where the adiabatic part is adjustable, along with a parallel canonical momentum formulation has been previously developed and benchmarked in simple geometry [6]. This is done in three-dimensional toroidal geometry using field-line-following coordinates [7]. The high-β problem in kinetic electron simulations with electromagnetic effects [6] has been solved recently [8]. We have also implemented a Monte-Carlo electron-ion collisional algorithm and the code has been linearly benchmarked in toroidal geometry with the continuum codes GS2 [9] and GYRO [10]. This particle simulation method can now model the electron dynamics with a time step only one-third smaller than the time step typically used in adiabatic electron simulations. In this paper we present representative simulation results on ITG turbulence and transport using this new capability. The simulations are performed for a model plasma with H-mode parameters, the Cyclone DIII-D Base Case [11]. Our focus here is on low-β, essentially electrostatic, simulations, however, the effects of magnetic field perturbations on ITG turbulence and transport due to finite-β are also discussed.

A second kinetic electron model based on closing zero-inertia drift-fluid equations has been developed [12, 13, 14] and progress is being made simulating electromagnetic turbulence. This model is now running in a three-dimensional toroidal flux-tube geometry and benchmarking with the fully kinetic electron code is underway. This algorithm addresses the physics regime of higher plasma beta, but not so high that compressional Alfven physics needs to be included. All the gyrokinetic simulation work reported here is being carried out jointly through a multi-institutional collaboration called the "Summit Framework." Summit is an open-source framework for both local and global massively parallel gyrokinetic turbulence simulations with kinetic electrons and electromagnetic perturbations [15]. This framework, written in Fortran 90, provides a unified object-based environment for sharing common components. Work is underway through Summit to include the kinetic electron models reported here, realistic magnetic geometry using quasi-ballooning coordinates [2] and global effects [16] under one software environment. This will allow the scientist to choose the physics components (and associated numerical advantages and disadvantages) most appropriate

for the given problem at hand.

The paper is organized as follows. In Section 2 the algorithm for simulating kinetic electrons with electromagnetic perturbations is summarized. In Section 3 the algorithm for the extended hybrid scheme that is to be included in the Summit Framework is described and the current status on code development is reported. Simulation results for the DIII-D base case using the kinetic electron model as described in Section 2 are presented in Section 4. A summary is given in Section 5.

2 Kinetic electron model

Three analytical/numerical techniques are used to make possible the direct simulation of kinetic electrons in three-dimensional geometry with electromagnetic perturbations. First, a canonical parallel momentum formulation [17] is used to eliminate numerical instabilities associated with finite-differencing of the $\partial A_\parallel/\partial t$ term in the parallel electric field, $E_\parallel = -\nabla_\parallel \phi - \partial A_\parallel/\partial t$. Second, a split-weight method [5, 6] is used for the electrons that permits larger timesteps. Third, careful numerical evaluation of the $(\omega_{\rm pe}^2/c^2)A_\parallel$ term that appears in Ampere's law in the canonical parallel momentum formulation (described in more detail below) permits accurate electromagnetic simulations at moderate beta.

We begin by briefly describing the canonical momentum formulation where $p_{\parallel\alpha} = v_{\parallel\alpha} + (q_\alpha/m_\alpha)\langle A_\parallel\rangle$ is used as a coordinate. The gyrokinetic equation is then

$$\frac{\partial f_\alpha}{\partial t} + \mathbf{v}_{\rm G\alpha}\cdot\nabla f_\alpha + \dot{p}_{\parallel\alpha}\frac{\partial f_\alpha}{\partial p_{\parallel\alpha}} = C(f_\alpha), \tag{1}$$

where $\alpha = i, e$,

$$\dot{p}_{\parallel\alpha} = \frac{q_\alpha}{m_\alpha}\tilde{\mathbf{b}}\cdot\nabla\langle\phi\rangle - \frac{\mu_\alpha}{m_\alpha}\tilde{\mathbf{b}}\cdot\nabla B + v_{\parallel\alpha}(\mathbf{b}\cdot\nabla\mathbf{b})\cdot\mathbf{v}_E + \frac{q_\alpha}{m_\alpha}\mathbf{v}_{\rm G\alpha}\cdot\nabla\langle A_\parallel\rangle, \tag{2}$$

$\mathbf{v}_{\rm G\alpha} = v_{\parallel\alpha}\tilde{\mathbf{b}} + \mathbf{v}_{\rm d\alpha} + \mathbf{v}_E$ is the guiding center velocity. $\tilde{\mathbf{b}} = \mathbf{b} + \dfrac{\langle\delta\mathbf{B}_\perp\rangle}{B}$, $\mathbf{v}_{\rm d\alpha} = \dfrac{v_\parallel^2 + v_\perp^2/2}{\Omega_\alpha B^2}\mathbf{B}\times\nabla B$ is the drift velocity for low β tokamak plasmas with $\beta \ll 1$, $\mathbf{v}_E = \langle\mathbf{E}\rangle\times\mathbf{b}/B$. The electrons are described by the drift-kinetic equations due to their small gyro radii, hence $\langle\phi\rangle = \phi$, etc., for electrons.

$C(f_\alpha)$ is a collision operator. We do not consider collision effects on ions, $C(f_i) = 0$, and use a Lorentzian operator for electrons, $C(f_e) = C_L(f_e)$:

$$C_L(f_e) = \nu_e \frac{1}{2}\frac{\partial}{\partial\lambda}(1-\lambda^2)\frac{\partial}{\partial\lambda} f_e \tag{3}$$

$$\nu_e = \frac{n_{0\mathrm{e}} e^4 \ln\Lambda}{4\pi\epsilon_0^2 m_e^2 v^3}\left(Z_{\mathrm{eff}} + H_{\mathrm{ee}}\left(\sqrt{m_e v^2/2T_{0\mathrm{e}}}\right)\right) \tag{4}$$

with $H_{\mathrm{ee}}(x) = \dfrac{e^{-x^2}}{\sqrt{\pi}x} + (1 - \dfrac{1}{2x^2})\mathrm{erf}(x)$.

The ions are simulated using the usual δf method. Define $f_i = f_{0\mathrm{i}} + \delta f_i$ with $f_{0\alpha}$ the Maxwellian distribution in $p_{\|\alpha}$ ($\varepsilon_\alpha = m_\alpha(v_{\perp\alpha}^2 + p_{\|\alpha}^2)/2$),

$$f_{0\alpha} = \frac{n_{0\alpha}}{(2\pi)^{3/2} v_{\mathrm{T}\alpha}^3} e^{-\varepsilon_\alpha/T_\alpha}, \tag{5}$$

where $m_\alpha v_{\mathrm{T}\alpha}^2 = T_{0\alpha}$. δf_i evolves according to

$$\frac{d\delta f_i}{dt} = -(v_{\|i}\frac{\delta\mathbf{B}_\perp}{B} + \mathbf{v}_E)\cdot\nabla f_{0\mathrm{i}} - \dot{\varepsilon}_i\frac{\partial f_{0\mathrm{i}}}{\partial\varepsilon_i} \tag{6}$$

where $\dot{\varepsilon}_i = \mu_i \mathbf{v}_{\mathrm{Gi}}\cdot\nabla B + m_i\, p_{\|i}\, \dot{p_{\|i}}$.

A fraction of the adiabatic part of the electrons perturbed distribution is treated separately in the split-weight scheme. Thus we write

$$f_e = f_{0\mathrm{e}} - \epsilon_g e\phi\frac{\partial f_{0\mathrm{e}}}{\partial\varepsilon_e} + h. \tag{7}$$

The distribution h evolves according to

$$\begin{aligned}\frac{dh}{dt} - C_L(f_e) \;=\; & -(v_{\|e}\frac{\delta\mathbf{B}_\perp}{B} + \mathbf{v}_E)\cdot\nabla f_{0\mathrm{e}} - \dot{\varepsilon_e}\frac{\partial f_{0\mathrm{e}}}{\partial\varepsilon_e} \\ & + \epsilon_g e(\frac{\partial\phi}{\partial t} + \mathbf{v}_{\mathrm{Ge}}\cdot\nabla\phi)\frac{\partial f_{0\mathrm{e}}}{\partial\varepsilon_e}.\end{aligned} \tag{8}$$

A Monte-Carlo scheme for the collision operator $C_L(f_e)$ is described in Section 4.

The electric potential ϕ and its derivative $\dot{\phi} = \partial\phi/\partial t$ are computed from the gyrokinetic Poisson equation [18],

$$n_{0\mathrm{i}}\frac{q_i^2}{T_{0\mathrm{i}}}(\phi - \tilde{\phi}) + \epsilon_g n_{0\mathrm{e}}\frac{e^2}{T_{0\mathrm{e}}}\phi = q_i\int \delta f_i\,\delta(\mathbf{R}+\boldsymbol{\rho}-\mathbf{x})\,d\mathbf{R}\,d\mathbf{v} - e\int h\,d\mathbf{v} \tag{9}$$

and its derivative

$$n_{0\mathrm{i}}\frac{q_i^2}{T_{0\mathrm{i}}}(\dot{\phi}-\dot{\tilde{\phi}}) = -\nabla\cdot\int q_i\, f_i\, \mathbf{v}_{\mathrm{Gi}}\, \delta(\mathbf{R}+\boldsymbol{\rho}-\mathbf{x})\; d\mathbf{R}\, d\mathbf{v} + \nabla\cdot\int e\, f_e\, \mathbf{v}_{\mathrm{Ge}}\; d\mathbf{v} \quad (10)$$

respectively. In Eq. 9 and Eq. 10 $\boldsymbol{\rho}$ is the vector leading from the gyro-center $\mathbf{R}$ to the particle position $\mathbf{x}$, $\tilde{\phi}$ is defined as

$$\tilde{\phi} = \sum_{\mathbf{k}} \Gamma_0(k_\perp^2 v_{\mathrm{Ti}}^2/\Omega_i^2)\phi_k\; \exp(i\mathbf{k}\cdot\mathbf{x}) \quad (11)$$

with $\phi = \sum_{\mathbf{k}} \phi_k \exp(i\mathbf{k}\cdot\mathbf{x})$. $\dot{\phi}$ and $\dot{\tilde{\phi}}$ are similarly defined.

The vector potential $A_\parallel$ is given by Ampere's law

$$\left(-\nabla_\perp^2 + \frac{\omega_{\mathrm{pe}}^2}{c^2}\right) A_\parallel = \mu_0 \left(q_i \int \delta f_i\, v_\parallel\, \delta(\mathbf{R}+\boldsymbol{\rho}-\mathbf{x})\; d\mathbf{R}\, d\mathbf{v} - e\int h v_\parallel\; d\mathbf{v}\right) \quad (12)$$

The $(\omega_{\mathrm{pe}}^2/c^2)A_\parallel$ term in this equation comes from the zero-order distribution $f_{0\mathrm{e}}$ which is Maxwelian in $p_\parallel$. In previous implementation of the split-weight scheme [6] which uses Eq. 12 directly it is found that at moderate β the Alfvén wave frequency and ITG mode growth rate deviate from the linear dispersion relation significantly. This problem can be solved by evaluating the $(\omega_{\mathrm{pe}}^2/c^2)A_\parallel$ term using the same marker particles and the same scattering operation as that used for the h term in Eq. 12. That is,

$$\frac{\omega_{\mathrm{pe}}^2}{c^2}A_\parallel \approx \beta_i \frac{V}{N}\tau \sum_j p_{\parallel \mathrm{j}}^2 A_\parallel(\mathbf{x}_j) S(\mathbf{x}-\mathbf{x}_j). \quad (13)$$

Here $\tau = T_{0\mathrm{i}}/T_{0\mathrm{e}}$, N is the number of electrons used in the simulation, V is the volume of the simulation box. $\beta_i = \mu_0 n_0 T_{0\mathrm{i}}/B_0^2$ is related to the total plasma β through $\beta = 2(1+1/\tau)\beta_i$. $S(\mathbf{x})$ is the particle shape function used to deposit particle current to neighboring grids. The resulting form of the Ampere's equation has a matrix that depends on the particle coordinates and time and is three-dimensional. The detailed algorithm will be presented elsewhere [8]. For very low β cases ($\beta_i m_i/m_e \ll 1$) that are essentially electrostatic Eq. 12 is used for better computational efficiency.

3 Kinetic electron extended hybrid algorithm

A hybrid simulation scheme that includes electromagnetic effects has been previously proposed and study in a slab geometry shows that it can ade-

quately simulate the shear Alfv́en waves and the finite beta effects on the ITG waves [12]. In this hybrid model ions are treated as gyrokinetic while electrons are described by fluid equations. Recently a kinetic electron closure valid for $\beta m_{\rm i}/m_{\rm e} \geq 1$ has been introduced [13, 14]. The new algorithm incorporates δf drift-kinetic electrons whose number-density moment is used to close the electron fluid momentum equation (Ohm's law). A toroidal extension of the hybrid algorithm has been formulated, and the code implementation is being validated. Two-dimensional slab test cases have examined small-amplitude kinetic shear-Alfvén waves with electron Landau damping, the ion-temperature-gradient instability, and the collisionless drift instability in an unsheared slab as a function of β [13]. The scheme, which is to be included as part of the Summit Framework, can be summarized as follows. The electron distribution function is given as $f_e = f_{0\rm e} + (\delta n_{\rm e}^{(0)}/n_{0\rm e}) f_{0\rm e} + h$, where $\delta n_{\rm e}^{(0)}$ is the lowest-order fluid component of the perturbed electron density. The total perturbed electron density $\delta n_e = \delta n_{\rm e}^{(0)} + \delta n_e^K$ ($\delta n_e^K = \int h d\mathbf{v}$) is obtained from the electron continuity equation deduced from the electron drift-kinetic equation. $A_\parallel$ is advanced in time according to $\partial A_\parallel/\partial t = -\nabla_\parallel \phi - E_\parallel$. $E_\parallel$ is obtained from the parallel Ohm's law which utilizes a kinetic closure for the electron pressure [19]: $\nabla P_{\parallel\rm e} = \nabla_\parallel P_{\parallel\rm e}^{(0)} + T_{\parallel e}^{(0)} \nabla_\parallel \delta n_{\rm e}^{(0)} + n_{0\rm e} \nabla_\parallel \delta T_{\parallel e}$ where $\nabla_\parallel \equiv \mathbf{b} \cdot \nabla$. $\nabla_\parallel (T_{\parallel \rm e}{}^{(eq)} + \delta T_{\parallel e}) = 0$ is imposed [19], $T_{\parallel \rm e}{}^{(eq)}$ is the equilibrium temperature (including gradients) and $P_{\parallel e}^{(0)} = n_{0\rm e} T_{\parallel \rm e}{}^{(eq)}$. Non-adiabatic kinetic corrections to the pressure moment are higher order in $(\omega/k_\parallel v_{\rm Te})^2$ than are the terms coming from the adiabatic response [11]. With the updated $A_\parallel$, Ampere's law determines the parallel electron current (needed for evolving the electron continuity equation): $e n_{0\rm e} u_{\parallel \rm e} = (1/\mu_0) \nabla_\perp^2 A_\parallel + \delta j_{\parallel \rm i}$, where $\delta j_{\parallel \rm i}$ is the perturbed parallel ion current. The electrostatic potential is obtained from the quasi-neutrality condition using the updated total electron and ion charge densities. Once $A_\parallel$ and ϕ are available, ion and electron coordinates and weights are evolved according to the ion gyrokinetic equation and the electron drift kinetic equation written in terms of h.

With electron inertia retained in the extended hybrid algorithm, the scheme is numerically unstable for $\beta_i m_i/m_e < 1$, because the Alfvén velocity then exceeds the electron thermal velocity and the electron response is therefore not adiabatic. For $k_\perp \rho_i > 1$, the value of β_i below which the extended hybrid algorithm is badly behaved increases. However, when the electron inertia is neglected in the electron fluid momentum balance (valid if the fluid response is dominantly adiabatic), the value of β_i below which the extended

hybrid algorithm is badly behaved decreases substantially. The kinetic extended hybrid scheme remains useful over an interestingly large range of β_i for including kinetic electron corrections when the electrons as a whole are dominantly adiabatic.

In sheared-slab configurations, the electron response transitions from hydrodynamic to resonant and lastly to adiabatic as a function of distance from the mode rational surface where $k_\parallel = 0$. Because the formal expansion of the kinetic extended electron hybrid equations is around an adiabatic fluid response like the expansion in Lin and Chen [20], this treatment is invalid in the resonance layer near the mode rational surface. When trying to simulate the ion-temperature-gradient instability in a sheared slab using the hybrid algorithm, we observed enhanced Alfvénic noise and growing modes (that saturated), but no easily identifiable ITG signal. In a torus the mode structure along the field line is finite in extent, and it is argued that the slab branch is not as important as the toroidal branch in driving transport because the radial scales of the slab branch are narrow. It remains to be investigated whether the hybrid algorithm is practical in toroidal configurations, and this effort is in progress.

4 Simulation results with kinetic electrons

In this section we present linear and nonlinear simulation results for a representative tokamak plasma, the DIII-D Cyclone Base Case [11]. We first summarize the geometry and computational method as follows. An equilibrium with concentric flux surfaces is assumed. The magnetic field strength is $B(r,\theta) = B_0(1-(r/R_0)\cos\theta)$. The field-line-following coordinates [7] (x,y,z) are defined by $x = r - r_0$, $y = (r_0/q_0)(q\theta - \zeta)$ and $z = q_0 R_0 \theta$. Here (r,θ,ζ) are the usual toroidal coordinates, R_0 is the major radius at the magnetic axis, r_0 is the minor radius at the center of the simulation domain, $q_0 = q(r_0)$ the safety factor. The size of the simulation box along the field line is $2\pi q_0 R_0$. Periodic boundary conditions are used in x and y, while the toroidal boundary condition [7] is used in z. A predictor-corrector scheme is used to advance particle coordinates and weights. The field equations Eq. 9, Eq. 10 and Eq. 12 are solved spectrally [6]. The Lorentz operator $C_L(f_e)$ is implemented as follows. From Eq. 7

$$C_L(f_e) = C_L(f_{0e}(p_\parallel)) - C_L(\epsilon_g \phi \frac{\partial f_{0e}}{\partial \varepsilon_e}) + C_L(h). \tag{14}$$

The ϵ_g term is nonlinear and will be neglected. The first term is given by,

$$C_L(f_{0e}(p_\parallel)) = -\tau\nu_e A_\parallel f_{0e}, \tag{15}$$

which is implemented as an additional term in the electron weight equation. The third term on the RHS of Eq. 14 is implemented using a Monte-Carlo method [21, 22],

$$\lambda_{\rm new} = \lambda_{\rm old}(1-\nu_e\delta t) \pm \left[\left(1-\lambda_{\rm old}^2\right)\nu_e\delta t\right]^{1/2}, \tag{16}$$

where $\pm$ means equal probability of $+$ or $-$ [21]. $\delta t = \triangle t$ for the corrector step and $\delta t = 2\triangle t$ for the predictor step, $\triangle t$ is the time step of the simulation.

In the following simulations we use the DIII-D base-case parameters: $R_0/L_n = 2.2$, $R_0/L_T = 6.9$, $T_{0i} = T_{0e}$, $r_0/R_0 = 0.18$, $q_0 = 1.4$, $\hat{s} = (r_0/q_0)(dq/dr) = 0.78$. Most of the simulation results are obtained with $\beta_i = 10^{-4}$. This small β_i is not important physically and the simulations are essentially electrostatic. However, the small but nonzero β_i allows an increased time step, possibly because the high frequency ω_H mode [23] is avoided. In all the simulations with kinetic electrons the mass ratio is $m_i/m_e = 1837$, the split-weight parameter is $\epsilon_g = 0.5$. Fig. 1 shows the growth rate and frequency of the $k_\theta\rho_i = 0.3$ mode as a function of R_0/L_T for $\nu_{ei} = 0$. Also shown are the results from the GS2 code with kinetic electrons. Very good agreement is seen between GS2 results and those from the split-weight particle code. For the base case $R_0/L_{Ti} = 6.9$, the linear growth rate with kinetic electrons is $\gamma L_n/v_{Ti} = 0.21$. The result obtained from simulations with adiabatic electrons is $\gamma L_n/v_{Ti} = 0.12$. In the kinetic electron simulation we can treat the passing electrons as adiabatic and follow only the trapped electrons. The growth rate thus obtained is very close to the kinetic electron result, hence the increase of the growth rate from the adiabatic electron result is mainly due to the nonadiabatic effect of the trapped electrons. Fig. 2 shows the mode growth rate as a function of $k_\theta\rho_i$ for the base case with $\nu_{ei}L_n/v_{Ti} = 0.136$. Results from both kinetic electrons and adiabatic electrons are shown. The results are obtained from linear simulations in which only a single k_θ mode is retained.

Fig. 3 shows the evolution of the ion heat diffusivity χ_i (ion heat flux $\left\langle \int d\mathbf{v}\hat{\mathbf{r}}\cdot\mathbf{v}_E\frac{1}{2}m_iv^2\delta f_i\right\rangle$ normalized by $1/L_{Ti}$) with $R/L_{Ti} = 6.9$, for three cases: (a) with kinetic electrons, $\beta_i = 10^{-4}$ and $\nu_{ei}L_n/v_{Ti} = 0.45$; (b) with adiabatic electrons; and (c) with kinetic electrons, $\beta_i = 0.002$ (corresponding to total plasma $\beta = 0.008$) and $\nu_{ei}L_n/v_{Ti} = 0.136$. The result for $\beta_i = 0.002$ will

be discussed later. The case (a) result is obtained with a simulation box of $l_x = l_y = 128\rho_i$ resolved by 128×128 grids in the $x-y$ plane. The number of grid points in the z direction is 32. A total of 16 777 216 particles per species is loaded, and a time step of $\triangle t\, \omega_{\rm ci} = 4$ is used. As can be seen from (a) and (b), with kinetic electrons the ion heat diffusivity is about $\chi_i/\rho_i v_{\rm Ti} = 0.01$, significantly increased from that with adiabatic electrons, $\chi_i/\rho_i v_{\rm Ti} = 0.0065$. This is roughly consistent with the increase in linear growth rates (See Fig. 2). As a result of the nonadiabatic effect of the electrons, a finite particle number flux is observed in the simulation corresponding to case (a), which is also shown in Fig. 3 (normalized by $1/L_{\rm Ti}$). The turbulent particle transport is intrinsically ambipolar (consistent with the assumption and use of the quasineutrality relation), with a diffusivity of about $D_i/\rho_i v_{\rm Ti} \approx 0.016$.

The nonlinear result with kinetic electrons in case (a) of Fig. 3 is converged with respect to the size of the simulation box and particle numbers. Fig. 4 shows the results of this convergence test. The cases shown are: (i) box size $l_x \times l_y = 64\rho_i \times 64\rho_i$, 4 194 304 particles per species; (ii) $l_x \times l_y = 128\rho_i \times 128\rho_i$, 8 388 608 particles per species; and (iii) $l_x \times l_y = 128\rho_i \times 128\rho_i$, 16 777 216 particles per species corresponding to case (a) in Fig. 3. Grid sizes are $\triangle x = \triangle y = \rho_i$, $\triangle z = l_z/32$. Time step $\omega_{\rm ci}\triangle t = 4$, $\nu_{\rm ei}/\omega_{\rm ci} = 10^{-3}$. One can see that convergence with respect to box size and particle number is achieved with a box size of $64\rho_i \times 64\rho_i$ and 32 particles per grid cell. In all the nonlinear simulations with kinetic electrons presented here a finite collision rate is used. It is observed that collisionless simulations with kinetic electrons do not saturate well. This might be indicative of a subtle role played by dissipation in gyrokinetic simulations, as pointed out by Krommes [24].

Since the turbulence-generated zonal flow plays an important role in regulating turbulence and transport [25], it is of interest to study the effects of kinetic electrons on the evolution of the Geodesic Accoustic Mode (GAM) and the residual zonal flow [26, 27]. Theory predicts no significant change due to kinetic electron effects. Fig. 5 shows the evolution of the GAM with kinetic electrons (the solid line) and adiabatic electrons (the dashed line). A scan of the residual zonal flow level with changing q is shown in Fig. 6, where the residual zonal flow level $\phi(\infty)/\phi(0)$ is plotted as a function of $h = \sqrt{\varepsilon}/q^2$ ($\varepsilon = r_0/R_0$). The line is predicted by the Rosenbluth-Hinton theory [26, 27] assuming adiabatic electrons. The simulation is initialized with a perturbed ion density while the perturbed electron density is set to zero. Only the $k_\theta = 0$ mode is retained and the simulation is linear. As can be seen

from Fig. 5 and Fig. 6 the residual level of the zonal flow is not significantly changed by kinetic electrons. This is consistent with the nonlinear results shown in Fig. 3, which shows an increase of the saturated ion heat flux that can be understood based on linear physics.

We now briefly discuss the finite-β effects on the ITG turbulence and transport. The frequency and growth rate of the $k_\theta \rho_i = 0.3$ mode as a function of plasma β for the base case is shown in Fig. 7. At low β, $\beta \leq 2\%$, the ITG branch dominates, while at higher β the Kinetic Ballooning Mode is dominant. As β is increased from zero the ITG modes becomes less unstable due to finite-β stabilization, and one expects that the saturated ion heat flux is also reduced from the electrostatic level. This can be seen from the $\beta = 0.8\%$ case in Fig. 3, which shows a saturated χ_i below the adiabatic electron level. The experimentally measured ion heat diffusivity for the DIII-D shot (shot #81499 at time t=4000ms, for which the base case parameters are based on) is $\chi_i = 3.5 \times 10^{-4}$ [11] in the unit of Fig. 3, much lower than the adiabatic electron level. Although a direct simulation of the experiment is not attempted here, as we do not yet have effects such as profile variation, realistic geometry, impurities, etc., in the model, the simulation results indicate that electromagnetic effects on the ITG turbulence play an important role in determining the transport level.

5 Summary

In this paper we present simulation results for the Ion-Temperature-Gradient-Driven turbulence and transport using the DIII-D Cyclone Base Case parameters [11]. The simulations use a δf gyrokinetic particle method that includes fully kinetic electrons, three-dimensional toroidal geometry using field-line-following coordinates and electromagnetic effects. Consistent with the increased linear growth rates of the ITG modes due to trapped electron drive, the saturated ion heat transport is increased from that obtained with adiabatic electrons. The evolution of zonal flows is not significantly changed by kinetic electrons, consistent with analytical theory [26, 27]. It is shown that finite-β stabilization of the ITG modes can effectively reduce the saturated ion heat transport. The code is implemented as part of the Summit Framework [15]. Summit is a collaborative effort aimed at both local and global massively parallel gyrokinetic turbulence simulations with kinetic electrons and electromagnetic perturbations. A hybrid model in which electrons

are treated by fluid equations with kinetic electron closure is also described.

Acknowledgements

This work is part of the Summit Framework, Computational Center for the Study of Plasma Microturbulence, an Office of Fusion Energy Sciences, United States Department of Energy, Scientific Discovery through Advanced Computing (SciDAC) Project. We thank Dr. W. Dorland for help with generating GS2 linear benchmarks.

References

[1] S. Parker, W. Lee, and R. Santoro, Phys. Rev. Lett. **71**, 2042 (1993).

[2] A. Dimits, T. Williams, J. Byers, and B. Cohen, Phys. Rev. Lett. **77**, 71 (1996).

[3] R. Sydora, V. Decyk, and J. Dawson, Plasma Phys. Controlled Fusion **38**, A281 (1996).

[4] Z. Lin, T. Hahm, W. Lee, W. Tang, and R. White, Science **281**, 1835 (1998).

[5] I. Manuilskiy and W. W. Lee, Phys. Plasmas **7**, 1381 (2000).

[6] Y. Chen and S. E. Parker, Phys. Plasmas **8**, 2095 (2001).

[7] M. A. Beer, S. C. Cowley, and G. W. Hammett, Phys. Plasmas **2**, 2687 (1995).

[8] Y. Chen and S. Parker, *submitted to J. Comput. Phys.* (2002).

[9] W. Dorland, F. Jenko, M. Kotschenreuther, and B. Rogers, Phys. Rev. Lett. **25**, 5579 (2000).

[10] J. Candy and R. Waltz, General Atomics Report GA-A23876, *to appear in J. Comput. Phys.*, (2002).

[11] A. Dimits et al., Phys. Plasmas **7**, 969 (2000).

[12] Y. Chen and S. E. Parker, Phys. Plasmas **8**, 441 (2001).

[13] B. I. Cohen, A. M. Dimits, W. Nevins, Y. Chen, and S. E. Parker, Phys. Plasmas **9**, 251 (2002).

[14] B. I. Cohen, A. M. Dimits, W. Nevins, Y. Chen, and S. E. Parker, Phys. Plasmas **9**, 1915 (2002).

[15] http://www.nersc.gov/scidac/summit .

[16] J. Leboeuf, V. Decyk, A. Dimits, and D. Shumaker, "Progress Towards Realistic Geometry and Global Implementations of the Summit Gyrokinetic Framework," Poster **1C10**, 2002 Int. Sherwood Fusion Theory Conf., Rochester, New York, USA, Apr. 22-24, (2002).

[17] T. S. Hahm, W. W. Lee, and A. Brizard, Phys. Fluids **31**, 1940 (1988).

[18] W. W. Lee, Phys. Fluids **26**, 556 (1983).

[19] P. Snyder, PhD thesis, Princeton University, 1999.

[20] Z. Lin and L. Chen, Phys. Plasmas **8**, 1447 (2001).

[21] A. H. Boozer and G. Kuo-Petravic, Phys. Fluids **24**, 851 (1981).

[22] Y. Chen and R. B. White, Phys. Plasmas **10**, 3591 (1997).

[23] W. Lee, J. Comput. Phys. **72**, 243 (1987).

[24] J. Krommes and G. Hu, Phys. Plasmas **1**, 3211 (1994).

[25] P. Diamond and Y. Kim, Phys. Fluids B **3**, 1626 (1991).

[26] M. N. Rosenbluth and F. L. Hinton, Phys. Rev. Lett. **80**, 724 (1998).

[27] F. L. Hinton and M. N. Rosenbluth, Plasma Phys. Controlled Fusion **41** (1999).

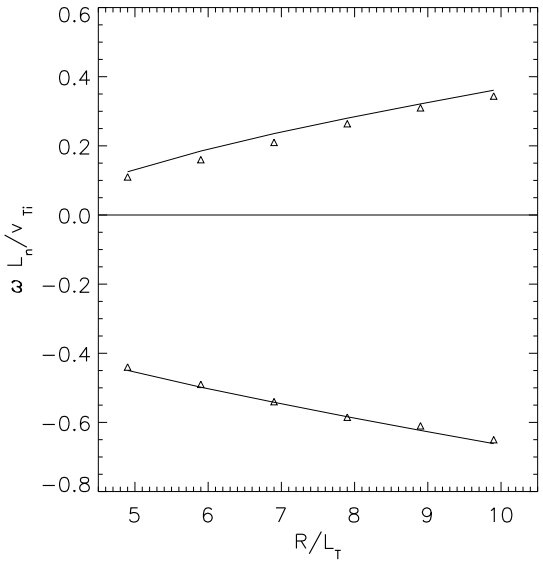

Figure 1: Growth rate and frequency of the $k_\theta \rho_i = 0.3$ mode vs. R/L_T, comparing the split-weight particle code with GS2. Upper part is for growth rates. Data points are from particle simulations.

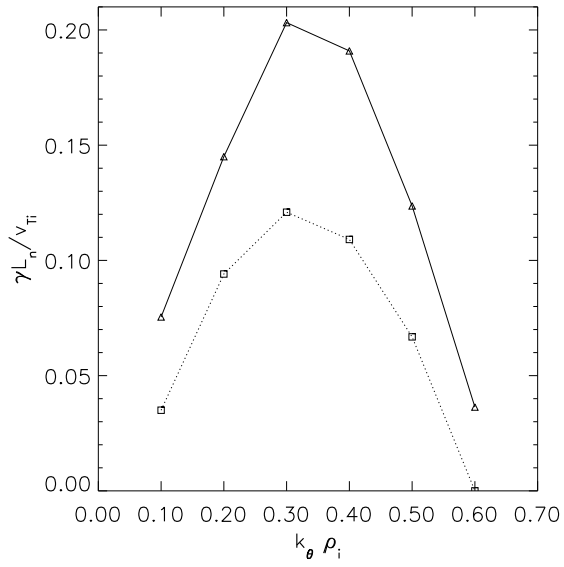

Figure 2: ITG mode growth rate vs. k_θ. Upper curve from kinetic electron simulations, lower curve from adiabatic electron simulations.

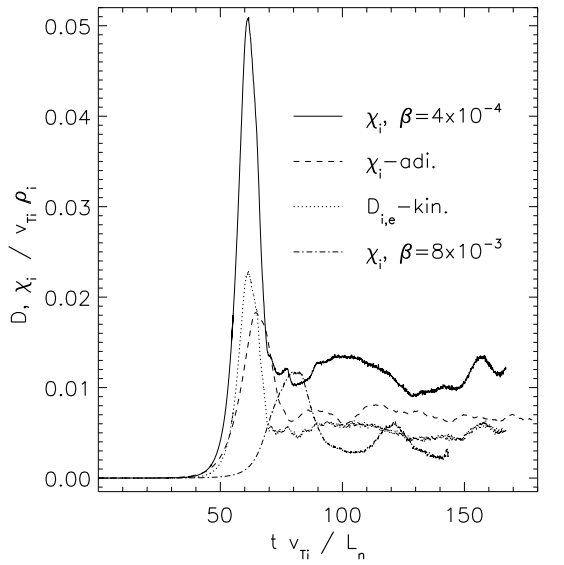

Figure 3: Evolution of the ion heat flux and particle diffusivity for the Base Case parameters.

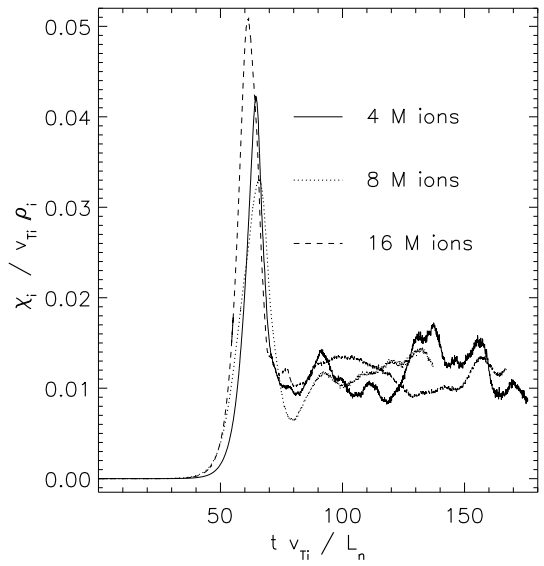

Figure 4: Convergence test with respect to particle number and box size.

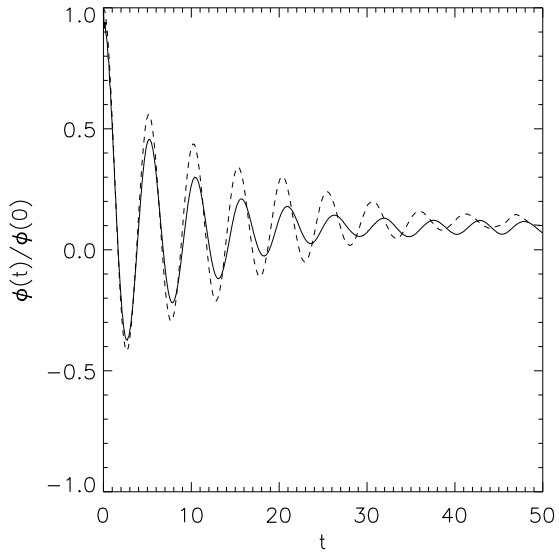

Figure 5: Evolution of the Geodesic Acoustic Mode and the residual zonal flow. Dashed line is obtained with adiabatic electrons, solid line with kinetic electrons.

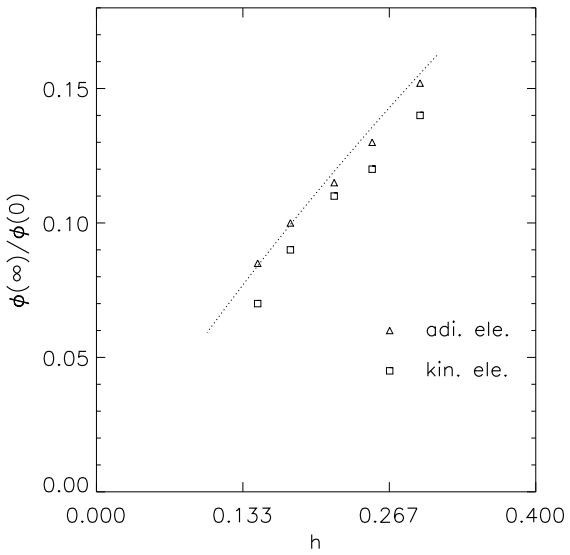

Figure 6: The residual level of the zonal flow versus magnetic shear. The line is predicted by Rosenbluth-Hinton theory.

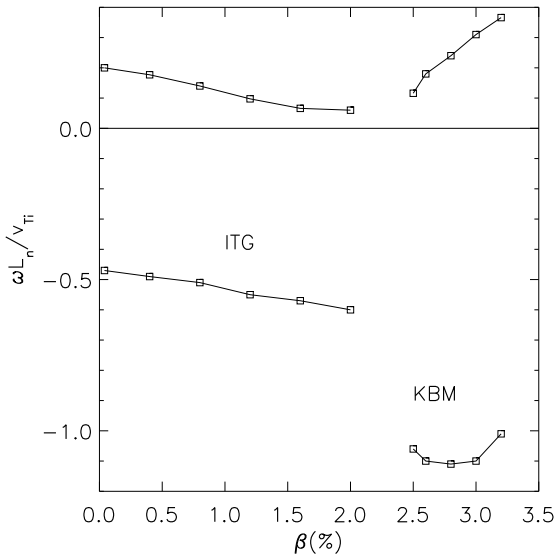

Figure 7: $k_\theta \rho_i = 0.3$ mode growth rate and frequency vs. β, showing the finite β stabilization of the ITG mode and the onset of the Kinetic Ballooning Mode. Upper part shows data for growth rates.